Coamplification of *miR-4728* protects *HER2*-amplified breast cancers from targeted therapy

Konstantinos V. Floros[a], Timothy L. Lochmann[a], Bin Hu[b], Carles Monterrubio[c,d], Mark T. Hughes[a], Jason D. Wells[e], Cristina Bernadó Morales[f,g], Maninderjit S. Ghotra[a], Carlotta Costa[h], Andrew J. Souers[i], Sosipatros A. Boikos[j], Joel D. Leverson[k], Ming Tan[l], Violeta Serra[g,m], Jennifer E. Koblinski[b], Joaquin Arribas[f,g,n,o], Aleix Prat[p], Laia Paré[p], Todd W. Miller[e], Mikhail G. Dozmorov[q], Hisashi Harada[a], Brad E. Windle[a], Maurizio Scaltriti[c,d], and Anthony C. Faber[a,1]

[a]Department of Oral and Craniofacial Molecular Biology, Philips Institute for Oral Health Research, VCU School of Dentistry and Massey Cancer Center, Virginia Commonwealth University, Richmond, VA 23298; [b]Department of Pathology, Virginia Commonwealth University School of Medicine, Richmond, VA 23220; [c]Department of Pathology, Memorial Sloan Kettering Cancer Center, New York, NY 10065; [d]Human Oncology & Pathogenesis Program, Memorial Sloan Kettering Cancer Center, New York, NY 10065; [e]Department of Molecular & Systems Biology, Norris Cotton Cancer Center, Geisel School of Medicine at Dartmouth, Lebanon, NH 03756; [f]Preclinical Research Program, Vall d'Hebron Institute of Oncology, 08035 Barcelona, Spain; [g]Centro de Investigación Biomédica en Red en Oncologia (CIBERONC), 08035 Barcelona, Spain; [h]Department of Medicine, Massachusetts General Hospital, Cancer Center and Harvard Medical School, Boston, MA 02129; [i]Oncology Discovery Department, AbbVie Inc., North Chicago, IL 60064; [j]Division of Hematology, Oncology and Palliative Care, Virginia Commonwealth University, Massey Cancer Center, Richmond, VA 23298; [k]Oncology Development Department, AbbVie Inc., North Chicago, IL 60064; [l]Department of Oncological Sciences, Mitchell Cancer Institute, University of South Alabama, Mobile, AL 36604; [m]Experimental Therapeutics Group, Vall d'Hebron Institute of Oncology, 08035 Barcelona, Spain; [n]Institució Catalana de Recerca i Estudis Avançats, 08010 Barcelona, Spain; [o]Department of Biochemistry and Molecular Biology, Universitat Autónoma de Barcelona, Campus de la UAB, 08193 Bellaterra, Spain; [p]Translational Genomics and Targeted Therapeutics in Solid Tumors, Institut D'Investigacions Biomèdiques August Pi i Sunyer, 08036 Barcelona, Spain; and [q]Department of Biostatistics, Virginia Commonwealth University, Richmond, VA 23298-0032

Edited by Jerry M. Adams, The Walter and Eliza Hall Institute of Medical Research, Melbourne, VIC, and approved January 25, 2018 (received for review October 11, 2017)

***HER2* (*ERBB2*) amplification is a driving oncogenic event in breast cancer. Clinical trials have consistently shown the benefit of HER2 inhibitors (HER2i) in treating patients with both local and advanced HER2+ breast cancer. Despite this benefit, their efficacy as single agents is limited, unlike the robust responses to other receptor tyrosine kinase inhibitors like EGFR inhibitors in *EGFR*-mutant lung cancer. Interestingly, the lack of HER2i efficacy occurs despite sufficient intracellular signaling shutdown following HER2i treatment. Exploring possible intrinsic causes for this lack of response, we uncovered remarkably depressed levels of NOXA, an endogenous inhibitor of the antiapoptotic MCL-1, in *HER2*-amplified breast cancer. Upon investigation of the mechanism leading to low NOXA, we identified a micro-RNA encoded in an intron of *HER2*, termed *miR-4728*, that targets the mRNA of the Estrogen Receptor α (*ESR1*). Reduced ESR1 expression in turn prevents ERα-mediated transcription of *NOXA*, mitigating apoptosis following treatment with the HER2i lapatinib. Importantly, resistance can be overcome with pharmacological inhibition of MCL-1. More generally, while many cancers like *EGFR*-mutant lung cancer are driven by activated kinases that when drugged lead to robust monotherapeutic responses, we demonstrate that the efficacy of targeted therapies directed against oncogenes active through focal amplification may be mitigated by coamplified genes.**

NOXA | apoptosis | *HER2* amplification | targeted therapies | MCL-1 inhibitor

Genetic amplification of the receptor tyrosine kinase (RTK) *HER2* (*ERBB2*) is found in breast cancers with amplification of the *17q12-21* locus, which occurs in 20–25% of invasive breast cancers. It has been demonstrated that trastuzumab, a humanized monoclonal antibody targeting HER2, when combined with chemotherapy, significantly improves progression-free survival (PFS) (7.4 vs. 4.6 mo) and overall survival (OS) (25.1 vs. 20.3 mo) (1) in patients with *HER2*-amplified breast cancer. A number of studies have since demonstrated that adjuvant use of HER2 kinase inhibitors, such as lapatinib, improves outcomes in *HER2*-amplified breast cancers, including reduced recurrence rates and increased OS (2). Interestingly, despite these clear benefits, HER2 kinase inhibitors used as monotherapy have demonstrated only minor benefit, with objective response rates (ORRs) below 20% (3). In contrast, other RTK-driven cancers like *EGFR*-mutant lung cancers (4) and *ALK*-translocated lung cancers (5) have ORRs approaching 60–70%.

Laboratory studies have indicated that EGFR, ALK, and HER2 inhibitors have comparable ability to block the critical PI3K/mTOR and MEK/ERK pathways (6, 7). This suggests that the poorer response rates of HER2 inhibitor monotherapy relative to those of EGFR and ALK inhibitors are not due to decreased inhibition of key intracellular signaling. Further downstream, these pathways converge on the BCL-2 family of proteins, which govern the ability of the cell to undergo apoptosis (8). The degree of apoptosis induced by targeted therapies is critical and directly influences targeted therapy responses (9–15). For instance, in response to MEK/ERK pathway inhibition, all three of these RTK-driven cancer subtypes up-regulate the expression of the proapoptotic, BH3-only BCL-2 family member, BIM. Loss of BIM expression universally protects these cancers from kinase inhibitor-induced apoptosis (6, 9, 14).

Interestingly, it is now appreciated that cancers with lower basal expression of functional BIM, either due to genetic polymorphisms (12) or other less defined causes (9, 11), are deficient

Significance

In *HER2*-amplified breast cancers, HER2 inhibitors have been very successful as adjuvant therapy but not as monotherapy. Here, we demonstrate that coamplification of a *HER2* intronic miRNA causes intrinsic resistance to HER2 inhibitors by indirectly down-regulating the pro-apoptotic NOXA. Importantly, coinhibition with MCL-1 inhibitors overcomes this resistance.

Author contributions: K.V.F. and A.C.F. designed research; K.V.F., B.H., C.M., M.T.H., J.D.W., C.B.M., M.S.G., V.S., J.E.K., J.A., A.P., L.P., and A.C.F. performed research; A.J.S., J.D.L., M.T., J.E.K., H.H., and A.C.F. contributed new reagents/analytic tools; K.V.F., T.L.L., B.H., C.C., A.J.S., S.A.B., J.D.L., V.S., J.E.K., A.P., L.P., T.W.M., M.G.D., H.H., B.E.W., M.S., and A.C.F. analyzed data; and K.V.F. and A.C.F. wrote the paper.

Conflict of interest statement: J.D.L. and A.J.S. are employees and shareholders of AbbVie Inc.

This article is a PNAS Direct Submission.

[1]To whom correspondence should be addressed. Email: acfaber@vcu.edu.

This article contains supporting information online at www.pnas.org/lookup/suppl/doi:10.1073/pnas.1717820115/-/DCSupplemental.

Published online February 23, 2018.

in an apoptotic response following kinase inhibitor treatment, even in the presence of MEK/ERK (and PI3K/mTOR) signal shutdown. Clinical studies have now been designed to overcome these BIM-centric deficiencies, by adding apoptosis-inducing agents to sensitize cancers to kinase inhibitors (16, 17).

In our investigations, we made the unexpected discovery that levels of NOXA (encoded by *PMAIP1*) were markedly low in breast cancers. We subsequently found that this phenomenon is strongly enriched in *HER2*-amplified breast cancers. As NOXA acts primarily as an endogenous inhibitor of the antiapoptotic BCL-2 family member MCL-1, we hypothesized that NOXA deficiency serves as a universal apoptotic block in *HER2*-amplified breast cancers, which could explain the lack of clinical HER2 inhibitor monotherapy activity. In this work, we tested this hypothesis and investigated the cellular mechanism(s) underlying this phenomenon.

Results

NOXA Is Uniformly Suppressed in *HER2*-Amplified Breast Cancer. Using gene expression datasets of cancer cell lines to understand the landscape of BCL-2 family member expression in breast cancer, we found that, within the cancer cell line encyclopedia (CCLE), levels of mRNA encoding the proapoptotic protein NOXA (*PMAIP1*) were markedly reduced in breast cancer cells compared with other cancer cell subtypes (Fig. S1) (18). Parsing multiple datasets (19–25) in the Oncomine database (26) and the R2 genomics application (r2.amc.nl), we found that *NOXA* mRNA levels were remarkably and specifically depressed in the *HER2*-amplified subset of breast cancer (Fig. 1*A*), while mRNA levels of other major proapoptotic BCL-2 family members were not depressed (Fig. S2*A*). We also found an inverse correlation

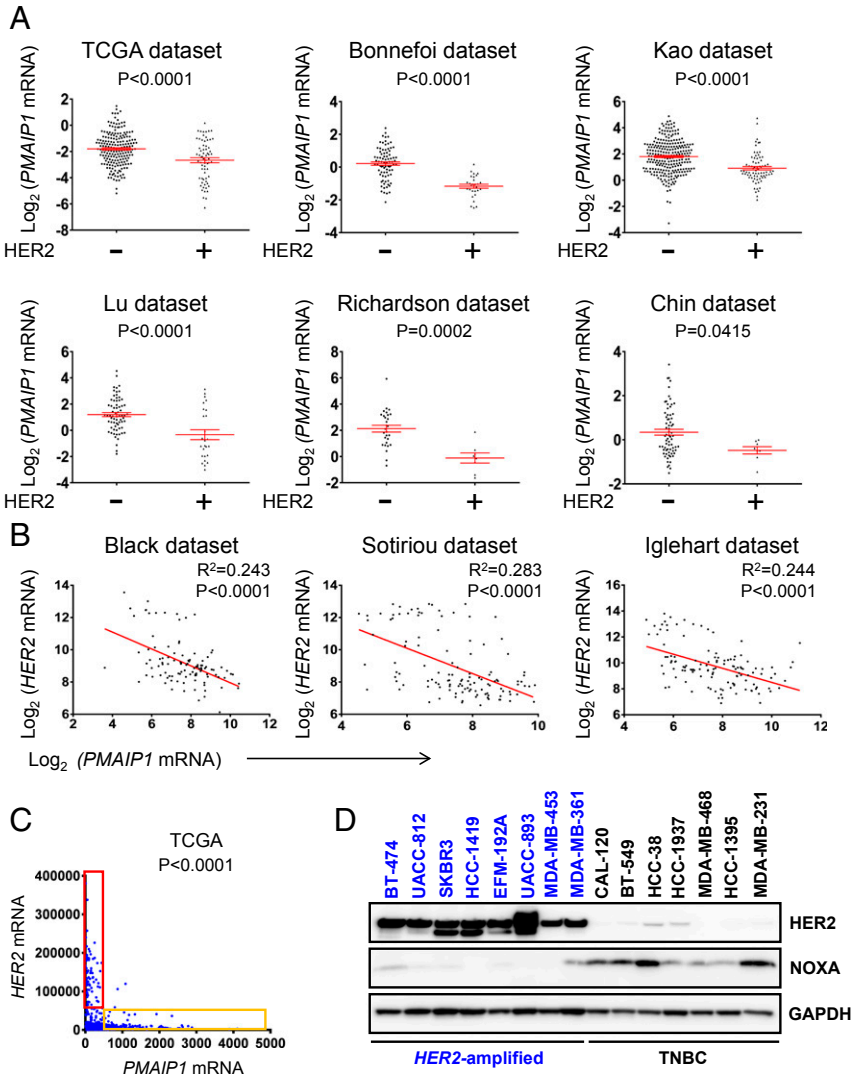

Fig. 1. NOXA (encoded by *PMAIP1*) is uniformly suppressed in *HER2*-amplified breast cancer. (*A*) Scatter plots comparing *PMAIP1* mRNA levels in *HER2*-amplified versus non-*HER2*–amplified breast cancers from six tumor databases of breast cancers obtained from Oncomine (https://www.oncomine.com/resource/login.html, May 2017, Thermo Fisher Scientific) (TCGA dataset: HER2−, $n = 194$; HER2+, $n = 67$; Bonnefoi dataset: HER2−, $n = 83$; HER2+, $n = 29$; Kao dataset: HER2−, $n = 252$; HER2+, $n = 75$; Lu dataset: HER2−, $n = 69$; HER2+, $n = 26$; Richardson dataset: HER2−, $n = 29$; HER2+, $n = 8$; Chin dataset: HER2−, $n = 71$; HER2+, $n = 8$). Red lines represent means. Error bars indicate ± SEM. (*B*) Scatter plots of *PMAIP1* mRNA expression against *HER2* mRNA expression from three datasets obtained from the R2 genomics application (r2.amc.nl) (Black dataset: $n = 107$; Sotiriou dataset: $n = 120$; Iglehart dataset: $n = 123$). (*C*) *HER2* (*ERBB2*) and *NOXA* (*PMAIP1*) mRNA expression correlation from 1,102 breast cancer tumors from TCGA. Red box indicates *NOXA* levels of high *HER2* cancers. Yellow box indicates *HER2* mRNA levels of tumors that have higher *NOXA* mRNA levels. *P* value was calculated using the Mann–Whitney *U* test (with *P* values < 0.05 equaling significance). (*D*) Untreated cells from a panel of *HER2*-amplified and TNBC cell lines were lysed and separated by SDS/PAGE, subjected to immunoblotting, and probed for HER2 or NOXA. GAPDH was used as a loading control.

between *HER2* and *NOXA* mRNAs in breast cancer (Fig. 1*B*). Consistently, from 1,102 breast cancer specimens deposited in The Cancer Genome Atlas (TCGA) (https://cancergenome.nih.gov/), we found a striking relationship between the highest HER2-expressing tumors and low NOXA expression (Fig. 1*C*). On the other hand, our analysis did not indicate a statistically significant relationship between *MCL1* and *HER2* mRNA (Fig. S2*D*). Furthermore, breast cancers determined to be HER2-positive (HER2+) by protein overexpression as measured by immunohistochemistry had significantly lower NOXA levels (Fig. S2*B*).

We next performed laboratory-based experiments to confirm the low levels of NOXA in *HER2*-amplified breast cancer and to understand the biological consequences of this deficiency. We first wanted to confirm that the mRNA expression results from the cell line and tumor datasets were reflected at the protein level. To investigate the expression levels of NOXA protein in *HER2*-amplified breast cancers, we interrogated whole-cell lysates from a panel of *HER2*-amplified and triple-negative breast cancer (TNBC) cell lines that were otherwise randomly selected. Consistently, the *HER2*-amplified breast cancer cell lines had markedly lower NOXA levels compared with the TNBC cell lines (Fig. 1*D*). Interestingly, BT-474 and MDA-MB-361 (HER2+)/(ER+) cell lines (27), which have elevated ERα protein levels among the HER2+ cell lines (Fig. S2*C*), demonstrated higher NOXA levels than the (HER2+)/(ER−) lines but lower levels than the TNBC cell lines. In contrast to NOXA, the key antiapoptotic proteins MCL-1 and BCL-xL did not exhibit expression patterns associated with HER2 status (Fig. S2*C*). Of note, while MCL-1 and BCL-xL were both expressed similarly in *HER2*-amplified and TNBC cell lines, the antiapoptotic protein BCL-2 was lower in most *HER2*-amplified cell lines (Fig. S2*C*), consistent with the mRNA data (Fig. S2*A*).

ER Status Affects NOXA Levels. To investigate whether ER status also impacted NOXA levels, we interrogated TCGA breast tumors in the Oncomine database (26). The lowest levels of NOXA mRNA expression were observed in the ER−/HER2+ subset of tumors, implying an association between both HER2 and NOXA and ER and NOXA (Fig. 2*A*). Consistently, within *HER2*-amplified breast cancers, ER− breast cancers had substantially lower levels of NOXA than ER+ breast cancers (Fig. 2*A*). These data indicate that both HER2 status and ER status correlate with NOXA levels. ER has been reported to directly up-regulate *NOXA* mRNA levels (28). In a different set of ER+ breast cancers (29), ER+ breast cancers demonstrated markedly higher NOXA levels compared with ER− tumors (Fig. 2*B*). In addition, when 22 HER2+ and 88 luminal A subtype breast cancers (29) [the latter are typically ER+/HER2− (30)] were compared, there was a striking difference in NOXA expression (Fig. 2*C*) (29). To determine whether there is also functional evidence to support these findings, we analyzed gene expression data from a clinical trial of presurgical treatment with the aromatase inhibitor letrozole, which suppresses estrogen biosynthesis to inhibit ER (31). Strikingly, NOXA was among the most significantly altered genes, markedly down-regulated after 14 d of letrozole treatment compared with baseline among 58 primary ER+ breast tumors

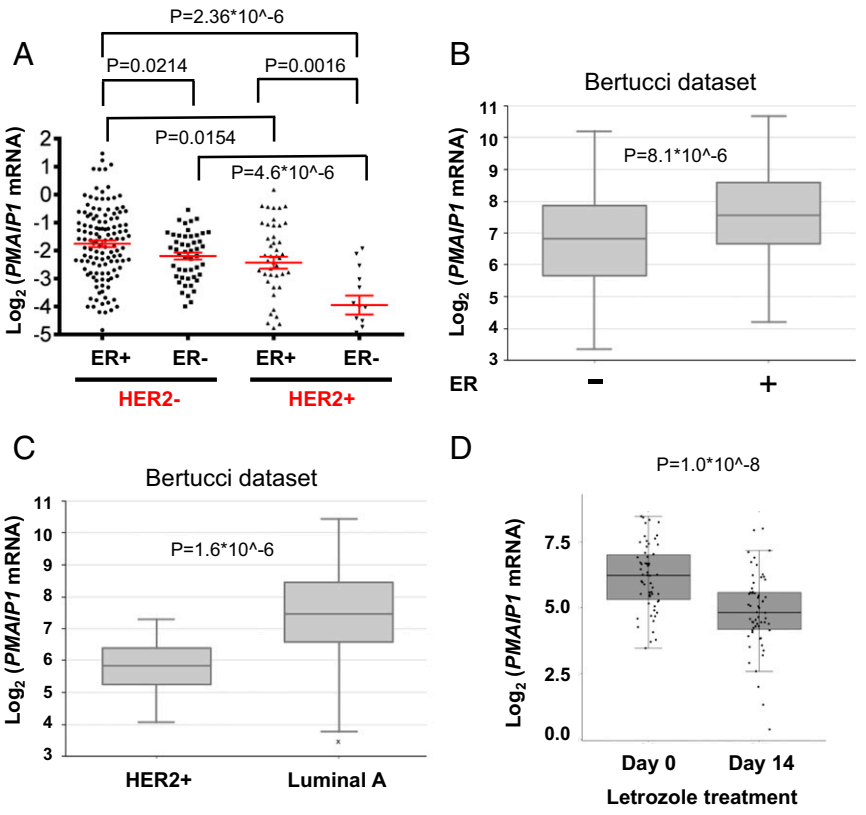

Fig. 2. *NOXA* mRNA expression is correlated with both ERα and HER2 in breast cancer. (*A*) Scatter plots comparing *PMAIP1* mRNA levels in HER2−/ER+, HER2+/ER−, ER−/HER2−, and ER+/HER2+ breast cancer tumors available for analysis from the TCGA obtained from Oncomine (https://www.oncomine.com/resource/login.html, May 2017, Thermo Fisher Scientific). Red lines represent means. The *P* values were calculated using the Mann–Whitney *U* test. (HER2−/ER+, $n = 126$; HER2+/ER−, $n = 14$; ER−/HER2−, $n = 49$; and ER+/HER2+, $n = 46$.) Error bars are SEM. (*B*) Box plot demonstrating differential *PMAIP1* mRNA expression levels between ER− ($n = 113$) and ER+ ($n = 150$) [as determined by immunohistochemistry (IHC)] breast cancers (29). *P* value was obtained from one-way ANOVA test. (*C*) Box plot demonstrating differential *PMAIP1* mRNA expression levels between HER2+ ($n = 22$) and luminal A breast cancers ($n = 88$). *P* value was obtained from one-way ANOVA test. (*D*) Box plot showing expression alteration (by fold change) of *NOXA* mRNA in ER+ breast tumor samples from 58 patients obtained at baseline and 14 d after presurgical treatment with letrozole (2.5 mg/d) (31).

(Fig. 2*D*). These data support the notion that ER drives NOXA expression in breast cancer.

Coamplification of *miR-4728* in *HER2*-Amplified Breast Cancer Leads to ER-Mediated Down-Regulation of NOXA. Our previous data showed a striking inverse relationship between HER2 and NOXA (Figs. 1 and 2 *A* and *C*). To gain insights into the mechanism that leads to NOXA deficiency in *HER2*-amplified breast cancers, we introduced siRNA targeting HER2 in three *HER2*-amplified breast cancer cell lines. Surprisingly, silencing HER2 did not affect NOXA mRNA levels (Fig. S3*A*). To further investigate a potential causative link between HER2 and NOXA, we analyzed the protein levels of NOXA in isogenic breast cancer cell lines with low (endogenous) vs. high (exogenous cDNA) HER2 (MCF7-GFP vs. MCF7-HER2) (32). Consistent with the siRNA analysis, we did not find that HER2 overexpression altered NOXA levels (Fig. S3*B*). We conclude that the expression of NOXA is independent of HER2 signaling. However, evidence in Figs. 1 and 2 suggested that NOXA expression is dependent on *HER2* amplification and HER2 expression; thus, there seems to be a contradiction.

We then investigated what would explain this seeming contradiction. Another potential mechanism by which NOXA may be down-regulated is through expression of micro-RNAs (miRNAs) that target the gene. Analyzing TCGA data from 964 tumors, we found that the top correlating miRNA with *HER2* mRNA, out of 1,626 miRNAs, is *miR-4728*, with a correlation coefficient of 0.7465 (Fig. 3*A*). These data led us to focus on *miR-4728*, which interestingly is located within intron 23 of the *HER2* gene and, as such, could be processed from the same primary transcript (33). Two mature miRNAs are formed from the precursor miR-4728—miR-4728-5p and miR-4728-3p—with miR-4728-3p being more prominently expressed as a mature miRNA (34). As previously mentioned, HER2 drives breast cancer formation as a focal amplicon manifesting as *17q12-21* amplification (35). An example of the amplicon in a *HER2*-amplified breast cancer from TCGA is depicted in Fig. S4*A*, illustrating the coamplification of *miR-4728*. Consistently, we found that the expression levels of *miR-4728-3p* in our panel of *HER2*-amplified breast cancers are much higher compared with the TNBC cell lines (Fig. 3*B*).

Importantly, it has recently been reported that *miR-4728* targets *ERα* (*ESR1*) mRNA (36, 37) and that ERα can function as a transcriptional factor for NOXA (28). Indeed, selective inhibition of ERα in BT-474 and MDA-MB-361 cells resulted in down-regulation of NOXA (Fig. S4*B*). Furthermore, our analyses indicated an inverse correlation between *ER* mRNA and *miR-4728*, which became apparent when we separated breast tumors by *miR-4728* expression: The highest *miR-4728* expressors had markedly low *ER* mRNA (Fig. 3*C*) as well as *NOXA* mRNA (Fig. 3*D*). We therefore hypothesized that when *HER2* is amplified in breast cancer, coamplification of *miR-4728* leads to down-regulation

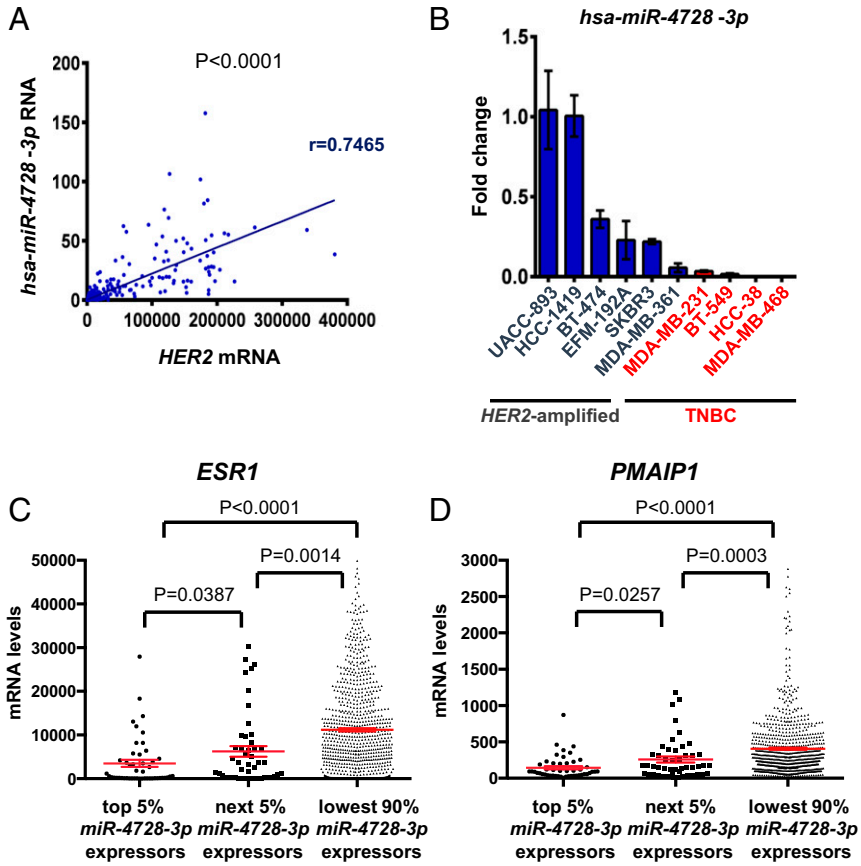

Fig. 3. *miR-4728* is coamplified and strongly correlated with HER2, while *NOXA* (*PMAIP1*) and *ERα* (*ESR1*) are inversely correlated with *miR-4728-3p* in breast cancer. (*A*) *HER2* (*ERBB2*) and *miR-4728* (*hsa-miR-4728*) correlation over 964 breast cancer tumors from TCGA. The Spearman correlation coefficient (r) and the *P* value (using Mann–Whitney *U* test) were calculated. (*B*) Total RNA enriched with small RNAs was isolated from a panel of *HER2*-amplified and TNBC cell lines. MiRNAs were reverse-transcribed using a TaqMan miRNA assay and finally analyzed by qPCR. *miR-26a-5p* was used as an endogenous control, and the data were expressed as a relative value to the cell line expressing the highest levels of *miR-4728-3p* (UACC-893); $n = 3$; error bars are ±SD. (*C*) Scatter plots comparing the *ESR1* mRNA levels in the top 5% *miR-4728* expressors versus the next 5% *miR-4728* expressors versus the lowest 90% *miR-4728* expressors from data analyses of 964 breast tumor samples. (*D*) Scatter plots comparing the *PMAIP1* (*NOXA*) mRNA levels in the top 5% *miR-4728* expressors versus the next 5% *miR-4728* expressors versus the lowest 90% *miR-4728* expressors from data analyses of 964 breast tumor samples. For (*C*) and (*D*), the red lines are means and the error bars are ± SEM.

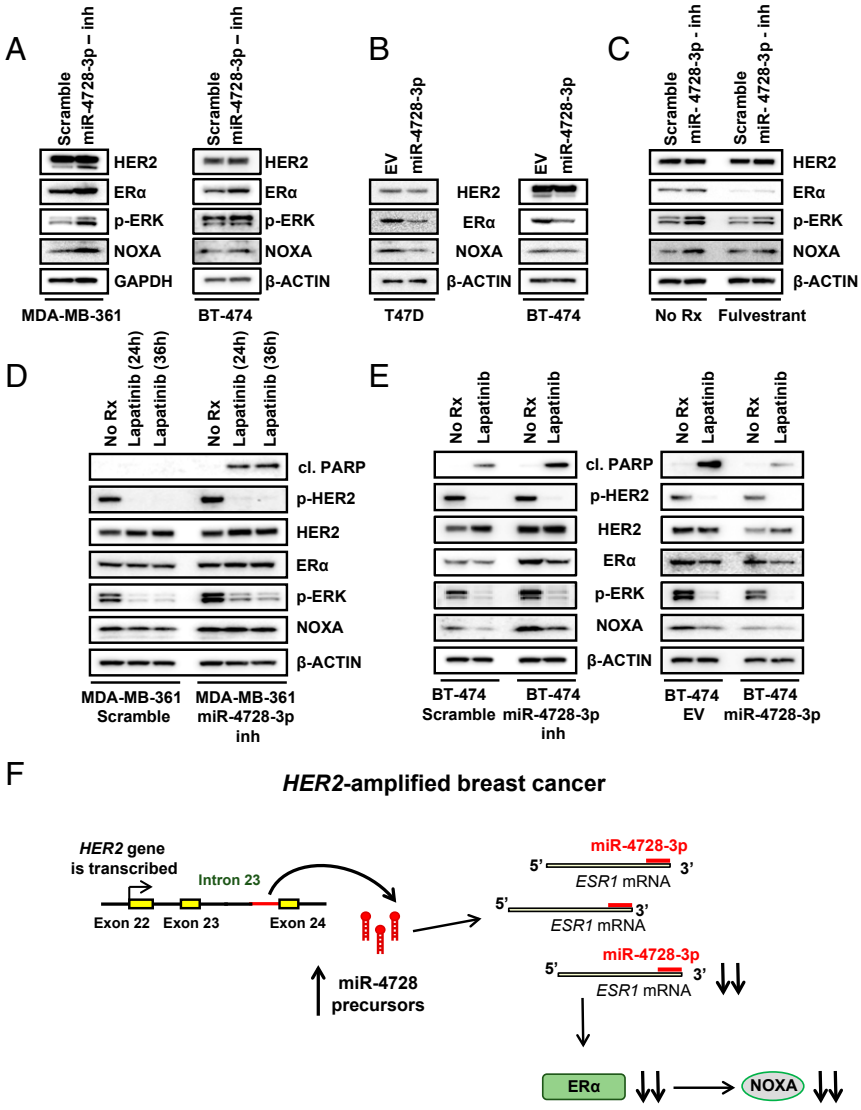

Fig. 4. Coamplification of *miR-4728* in *HER2*-amplified breast cancer causes ERα-mediated NOXA down-regulation and its inhibition sensitizes them to lapatinib, while its overexpression rescues lapatinib-treated *HER2*-amplified breast cancer cells from apoptosis. (*A*) The indicated *HER2*-amplified breast cancer cell lines were transfected with the pLV-hsa-miR-4728-3p locker plasmid (miR-4728 inhibitor) or control plasmid expressing a scrambled sequence (vector control), and the corresponding lysates were subjected to immunoblotting for NOXA, ERα, HER2, and phospho-ERK. GAPDH and β-ACTIN were used as loading controls. (*B*) The indicated breast cancer cell lines were infected with control vector or a mir-4728 overexpressing construct, and the corresponding lysates were subjected to Western blotting and probed for NOXA, ERα, HER2, and β-ACTIN (loading control). (*C*) MDA-MB-361 cells were transfected with the appropriate constructs, as in *A*, treated with no drug or 200 nM fulvestrant for 24 h and probed for the indicated proteins. β-ACTIN was used as a loading control. (*D*) MDA-MB-361 cells were transfected as in *A* and treated with no drug and with 1 μM of lapatinib for the indicated time points. The corresponding lysates were subjected to Western blotting and probed for the indicated proteins. β-ACTIN was used as a loading control. (*E*) BT-474 cells were transfected with the pLV-hsa-miR-4728-3p locker plasmid (miR-4728 inhibitor) or control plasmid expressing a scrambled sequence (vector control), treated with no drug or 1 μM lapatinib for 24 h. The corresponding lysates were subjected to Western blotting and probed for the indicated proteins. β-ACTIN was used as a loading control. BT-474 cells were also infected with control vector or a miR-4728–overexpressing construct, like in *B*, and treated with no drug or 1 μM lapatinib for 36 h. The corresponding lysates were subjected to Western blotting and probed for the indicated proteins. (*F*) Suggested model for NOXA regulation by the *HER2* amplicon in breast cancer. *miR-4728-3p* is coamplified with its host gene (*HER2*) and proceeds to silence *ESR1* expression. ERα encoded by *ESR1* functions as a transcriptional factor of NOXA; therefore, miR-4728 coamplification leads to down-regulation of NOXA ("No Rx": No drug).

of ER and NOXA, resulting in a mitigated response to HER2 inhibitors through the MCL-1 function.

We inhibited *miR-4728-3p* after transfection of MD-MB-361 and BT-474 cells with a specific pLV-hsa-miR-4728-3p locker plasmid or a scrambled vector control (38). As demonstrated in Fig. 4*A*, we observed a concomitant increase of estrogen receptor α (ERα), the dominant ER isoform in breast cancer (39), and of NOXA. Of note, the phosphorylation status of ERK served as a positive control for miR-4728 inhibition (38). In contrast, overexpression of miR-4728-3p in T47D (HER2−/ER+) and BT-474 (HER2+/ER+) cells was sufficient to decrease both ERα and NOXA (Fig. 4*B*). The increased expression levels of *miR-4728-3p*, in our overexpression models, were verified by qPCR analysis (Fig. S4*C*). Moreover, inhibition of ERα with a selective antagonist (fulvestrant) (40) mitigated the effect of pLV-hsa-miR-4728-3p locker plasmid on NOXA induction in MDA-MB-361 cells (Fig. 4*C*). We then tested whether inhibition of *miR-4728* sensitizes *HER2*-amplified breast cancer cells to the HER2 inhibitor, lapatinib. Indeed, MDA-MB-361 as well as BT-474 cells transfected with the pLV-hsa-miR-4728-3p locker plasmid demonstrated markedly elevated cleaved PARP compared with the control

cells (Fig. 4 *D* and *E*), while overexpression of *miR-4728* in BT-474 cells rescued lapatinib-treated cells from apoptosis (Fig. 4*E*). Altogether, these data demonstrate that *miR-4728* coamplification results in ER silencing, which in turn prevents expression of NOXA (28). Our model is depicted in Fig. 4*F*.

Pharmacological Inhibition of MCL-1 Sensitizes *HER2*-Amplified Breast Cancer Cells to Lapatinib. Altogether, our data indicate that coamplification of *miR-4728* plays a heretofore undiscovered role in *17q12-21* amplified breast cancer and that deficient expression of the intrinsic MCL-1 inhibitor NOXA may lead to an underlying apoptotic block in *HER2*-amplified breast cancers. To determine whether NOXA expression confers sensitivity to HER2 inhibition, we first artificially increased the levels of NOXA by transducing viral particles containing a NOXA-expressing plasmid into *HER2*-amplified breast cancer cells, treating the cells with a time course of lapatinib (Fig. 5*A*). Consistent with our hypothesis, NOXA-expressing cells were markedly sensitized to lapatinib, compared with control cells, as evidenced by increased PARP cleavage in HCC-1419 and MDA-MB-453 cells (Fig. 5*A*), as well as in EFM-192A and

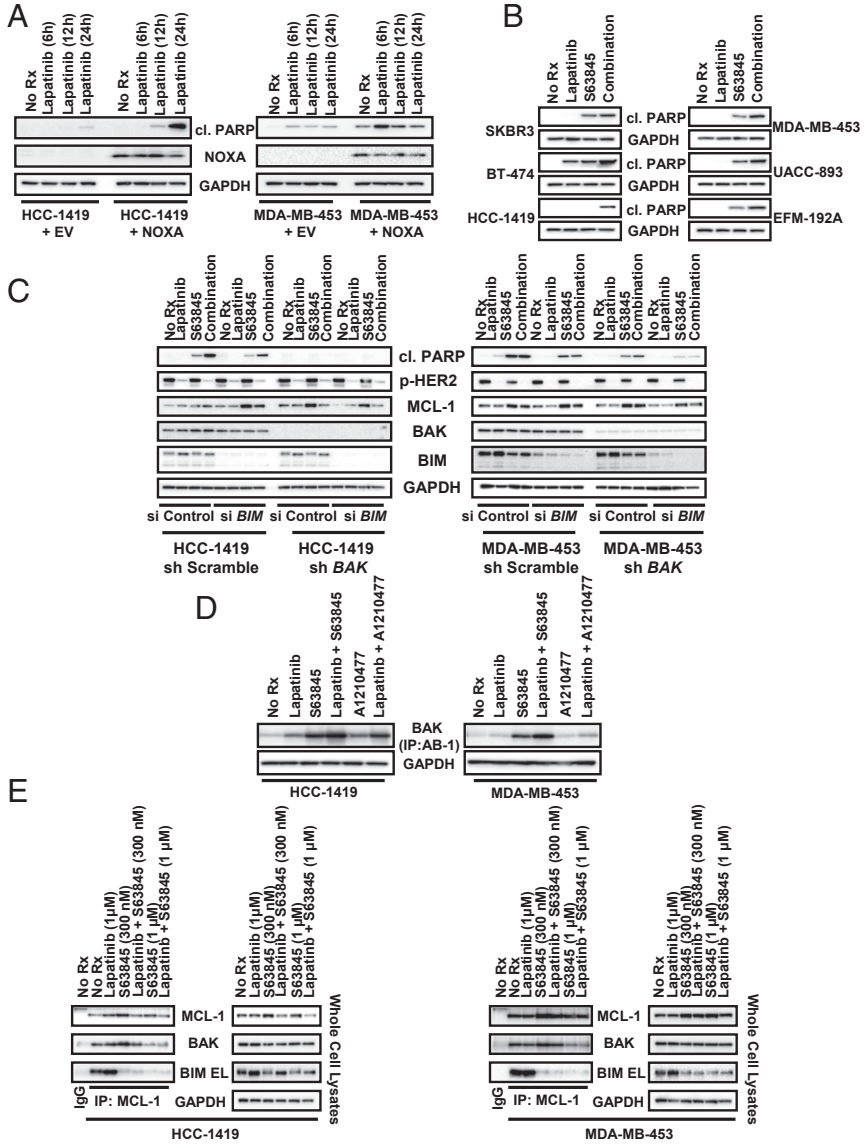

Fig. 5. S63845 sensitizes *HER2*-amplified breast cancer cells to lapatinib. Proapoptotic BCL-2 proteins BIM and BAK are required for the function of S63845, which selectively displaces BIM and BAK from MCL-1. (*A*) HCC-1419 and MDA-MB-453 cells were transduced with lentivirus containing an empty vector or a NOXA-expressing plasmid and treated with no drug or 1 μM lapatinib for 6, 12, and 24 h. Whole-cell lysates were prepared and subjected to Western blotting and probed for cleaved PARP, NOXA, and GAPDH. (*B*) A panel of *HER2*-amplified breast cancer cell lines were treated with lapatinib with or without 1 μM S63845 for 3 h (SKBR3, BT-474, and UACC-893) or for 8 h (MDA-MB-453, HCC-1419, and EFM-192A), and the expression levels of cleaved PARP were detected by Western blotting. (*C*) The stable cell lines described in D were treated with 50 nM scrambled or BIM-targeting siRNA for 24 h. Cells were reseeded and treated the following day with no drug, 1 μM lapatinib, 1 μM S63845, and their combination overnight. Cell lysates were prepared and subjected to Western blotting and probed for cleaved PARP, BAK, phospho-HER2, MCL-1, BIM, and GAPDH. (*D*) HCC-1419 and MDA-MB-453 cells were treated with no drug, 1 μM lapatinib, 10 μM A1210477, 1 μM S63845, and their combinations (A1210477/lapatinib and S63845/lapatinib) overnight, and CHAPS lysates were prepared and subjected to AB-1 IP and Western blotting. Total cell lysates were analyzed in parallel. (*E*) MCL-1 complexes were immunoprecipitated from the indicated *HER2*-amplified breast cancer cell lines following overnight treatment with no drug, lapatinib, S63845, and their combination at the indicated drug concentrations. An IgG-matched isotype antibody was served as an immunoprecipitation control. The interaction between MCL-1 and BIM/BAK proteins was investigated ("No Rx": No drug).

MDA-MB-361 cells (Fig. S5*A*). Immunoprecipitation analysis of these lysates revealed that MCL-1:BIM and MCL-1:BAK complexes were reduced by NOXA overexpression, consistent with the understanding of NOXA as an endogenous MCL-1 inhibitor (41) (Fig. S5 *B* and *C*). To further confirm this effect of NOXA expression, we reduced MCL-1 expression with a siRNA targeting MCL-1 (15) or a siRNA with a scrambled sequence and treated *HER2*-amplified HCC-1419 and MDA-MB-453 breast cancer cells with lapatinib. As expected, we found that the cells treated with siRNA targeting MCL-1 were markedly sensitized to lapatinib compared with the scramble siRNA-treated cells (Fig. S5*D*). These data indicate that NOXA overexpression confers sensitivity to HER2 inhibitors in *HER2*-amplified breast cancers.

Due to the emerging role of MCL-1 in cancer development, progression, and cell survival (42), MCL-1 inhibitors are being heavily pursued as anticancer agents. A1210477 is a BH3 mimetic that has been described to bind with high affinity to MCL-1 and selectively disrupts the interaction between proapoptotic BIM and MCL-1 (43). We therefore tested A1210477 in combination with lapatinib. Our data revealed that the addition of A1210477 effectively reduced the apoptotic threshold and markedly sensitized *HER2*-amplified breast cancer cells to lapatinib, as evidenced by cleaved PARP induction (Fig. S6*A*). The increased amount of apoptosis from the combination of lapatinib and A1210477 translated to enhanced sensitivity in 72-h cell viability assays (Fig. S6*B*). To further confirm the mode of activity of A1210477, we treated additional *HER2*-amplified breast cancer cell lines with lapatinib, A1210477, or the combination and evaluated the status of the major intracellular signaling pathways downstream of HER2 (6, 44). As expected, A1210477 did not alter the PI3K/mTOR or MEK/ERK pathways (Fig. S7), indicating that its sensitizing effects were specific to MCL-1 inhibition.

To better understand the mechanism linking sensitization of the *HER2*-amplified breast cancer cells to A1210477, we immunoprecipitated MCL-1 complexes in HCC-1419 and MDA-MB-453 cells. As expected, addition of A1210477 disrupted the interaction between MCL-1 and BIM (45) (Fig. S8*A*), releasing BIM to activate the effector molecules BAX and BAK and induce apoptosis (46–50). Furthermore, it is worth noting that lapatinib and A1210477 increased BIM and MCL-1 levels, respectively, consistent with previous reports (43, 51). The consequence of these increases was, at least in part, the accumulation of MCL-1:BAK complexes (Fig. S8*A*). To further study the roles of BIM and BAK in lapatinib/A1210477-mediated apoptosis, we stably knocked down BAK (sh*BAK*) in the same *HER2*-amplified breast cancer cell lines (HCC-1419 and MDA-MB-453) and silenced BIM with siRNA. In both cell lines, there was a clear requirement for both BIM and BAK in lapatinib/A1210477-mediated cell death, with the HCC-1419 cells particularly reliant on BAK (Fig. S8*B*).

The MCL-1 Inhibitor S63845 Synergizes with Lapatinib by Disrupting both MCL-1:BAK and MCL-1:BIM Complexes in *HER2*-Amplified Breast Cancers. The addition of A1210477 to lapatinib appeared effective because low NOXA caused the increase in MCL-1:BIM complexes, and A1210477 disrupted these complexes, therefore increasing the amount of liberated BIM. This is a critical step in apoptosis caused by kinase inhibitors and BCL-2 family inhibitors (8, 9, 15, 52–55). However, A1210477 did not robustly disrupt MCL-1:BAK complex formation (Fig. S8*A*). The new selective MCL-1 inhibitor, S63845, reportedly disrupts both BIM:MCL-1 and BAK:MCL-1 complexes (45), which may be a result of higher affinity for binding to the MCL-1 hydrophobic pocket than A1210477 (56). We first combined lapatinib with S63845 and found that the combination potently induced apoptosis as evidenced by cleaved PARP (Fig. 5*B*) and FACS analysis of annexin V-stained cells (Fig. S9*A*). Additionally, the combined treatment reduced viable cell numbers in *HER2*-amplified breast cancer cells (Fig. S9*B*). Intriguingly, in some of the cell lines (BT-474 and UACC-893), the combination of the two drugs displayed remarkable synergism, leading to robust cell death in less than 24 h (Fig. 5*B* and Fig. S9*B*). To ensure that S63845 functions exclusively through MCL-1 inhibition, we immunoprecipitated BIM complexes in both BT-474 and UACC-893 cells and found that addition of S63845 disrupts only the BIM:MCL-1 and not the BIM:BCL-xL or the BIM:BCL-2 complex (Fig. S10*A*). As in the case of A1210477, S63845 leaves PI3K/mTOR and MEK/ERK signaling unperturbed (Fig. S10*B*), confirming previously published data (57).

We next examined the requirement for BIM and BAK in lapatinib-, S63845-, and S63845/lapatinib-mediated toxicity in the *HER2*-amplified HCC1419 and MDA-MB-453 cells. Similar to the data with A1210477, knockdown of both BIM and BAK substantially mitigated drug-induced toxicity in the cells, with knockdown of BAK alone markedly protecting HCC1419 cells (Fig. 5*C*). Consistently, knockdown of BAK and BIM translated to significantly increased cell viability following treatment compared with controls (Fig. S11*A*). We next investigated any involvement of BAX in drug-induced toxicity. Knockdown of BAX expression with sh*BAX* also protected cells from MCL-1i/lapatinib-induced toxicity, albeit to a lesser degree than BAK (Fig. S11*B*). Interestingly, the protective effects of BAX and BIM appear redundant, as knockdown of BIM in the presence of knockdown of BAX did not markedly increase the amount of protection in either cell line (Fig. S11*B*). Using specific antibodies that recognize the active conformation of BAK or BAX (clone AB-1 for BAK or clone 6A7 for BAX, respectively) (58, 59), we immunoprecipitated lysates from HCC-1419 and MDA-MB-453 cells treated overnight and individually with lapatinib, A1210477, and S63845 or the combinations of lapatinib/A1210477 and lapatinib/S63845, with the AB-1 and 6A7 antibodies. Consistently, we detected levels of both active BAK and BAX following drug exposure that were generally much more pronounced in the combination treatments compared with single agents (Fig. 5*D* and Fig. S11*C*).

To verify that both MCL-1:BIM and MCL-1:BAK complexes were disrupted by S63845, we immunoprecipitated MCL-1 complexes in lysates of the *HER2*-amplified breast cancer cells, HCC-1419 and MDA-MB-453, following treatment with lapatinib, S63845 (at two concentrations of 300 nM and 1 μM), or their combination (Fig. 5*E*). Immunoprecipitation complex investigation confirmed that both MCL-1:BIM and MCL-1:BAK complexes were disrupted following treatment with 1 μM of S63845. These data imply that S63845-induced apoptosis involves disruption of BIM:MCL-1 and BAK:MCL-1 complexes in *HER2*-amplified breast cancer cells.

We next analyzed lysates from these *HER2*-amplified breast cancer cells to assess dependence upon the three main antiapoptotic BCL-2 family proteins for survival, following HER2 inhibition. Treatment with the combination of lapatinib/S63845 led to a marked increase in PARP cleavage, compared with lapatinib/A1331852 (a BCL-xL inhibitor) or lapatinib/venetoclax (a BCL-2 inhibitor) (Fig. S12*A*). However, knocking down BAK in HCC-1419 and MDA-MB-453 cells conferred resistance to MCL-1 inhibition (Fig. S12*B*).

Combination Treatment with Lapatinib and S63845 Consistently Induces Tumor Regression. To expand and corroborate our findings in vivo, BT-474 xenografts were established in NOD SCID gamma (NSG) female mice, and mice were treated with 100 mg/kg of lapatinib, 25 mg/kg of S63845, or their combination, for 5 consecutive days as previously described (60). Both drugs showed modest efficacy as single agents and variably slowed tumor growth or induced modest regression. However, the combination led to marked regression of 10/10 tumors (Fig. 6*A* and Fig. S13*A*). Cleaved PARP was up-regulated following combination drug treatment (Fig. 6*B*), indicating cell death. Furthermore, we assessed the drug treatments in a HER2+/ER− breast cancer patient-derived xenograft (PDX) model via injection into NSG mice following the same dosing schedule. Again, the single agents displayed modest activity, inhibiting tumor growth, whereas the combination shrank most of the tumors,

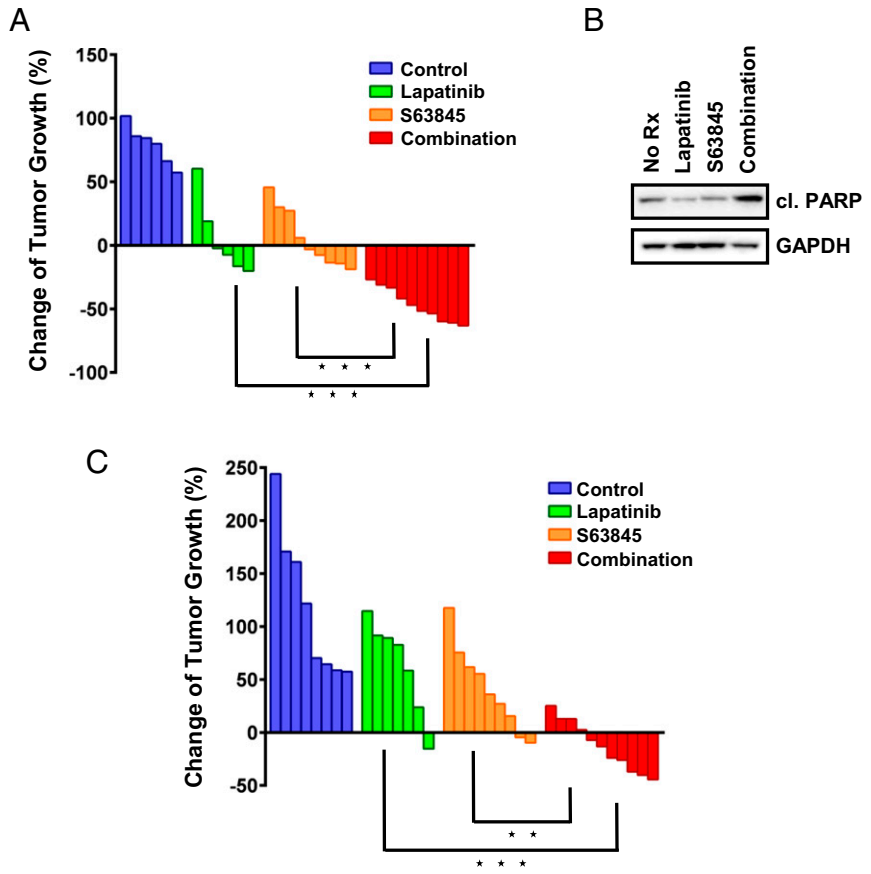

Fig. 6. Combination treatment with lapatinib and S63845 leads to antitumor activity in vivo. (*A*) Approximately 15×10^6 BT-474 cells were injected orthotopically into each NSG mouse (both sides) and monitored for subsequent growth. After tumors reached a size of ~150 mm^3, mice were treated with 25 mg/kg S63845, 100 mg/kg lapatinib, or the combination for 5 consecutive days. Tumor measurements were performed every day by calipers, and the percentage (%) of changes in volume for each tumor is shown by a waterfall plot (control, 6 tumors; lapatinib, 6 tumors; S63845, 9 tumors; combination, 10 tumors). *P* values were calculated using the Student *t* test. (*B*) Tumors were harvested from BT-474 tumor-bearing mice ~2 h after lapatinib administration, and tumor lysates were subjected to Western blot analyses and probed for cleaved PARP and GAPDH ("No Rx": No drug). (*C*) Approximately 1.5×10^6 cells derived from a PDX breast cancer model were injected orthotopically into each NSG mouse (both sides) and monitored for subsequent growth. After tumors reached a size of 150–200 mm^3, mice were treated with 25 mg/kg S63845, 100 mg/kg lapatinib, or the combination for 5 consecutive days. Tumor measurements were performed every day by calipers, and the percentage (%) of changes in volume for each tumor is shown by a waterfall plot (control, 8 tumors; lapatinib, 7 tumors; S63845, 9 tumors; combination, 11 tumors). *P* values were calculated using the Student *t* test.

similar to the BT-474 xenograft model (Fig. 6*C* and Fig. S13*B*). Immunohistochemistry detection of cleaved caspase-3 confirmed induction of apoptosis in a PDX tumor treated with S63845, with more pronounced apoptosis seen with the combination (Fig. S13*C*), consistent with the in vitro data (Fig. 5). Altogether, these data indicate that the *miR-4728*–ERα–NOXA pathway can be successfully targeted by cotreatment of HER2 inhibitors together with MCL-1 inhibitors.

Discussion

Breast cancers with amplification of *17q12-21* are driven by, and addicted to, HER2 (60). In genetically engineered mice, HER2 expression driven by the *MMTV* promoter is sufficient to cause the development of multiple invasive mammary carcinomas, and tumor regressions follow inactivation of *MMTV-HER2* in these mice (61). Follow-up studies in these mouse models focused on the proapoptotic BH3-only protein BIM, the abundance of which was increased upon HER2 inhibition. When HER2 was inactivated in *MMTV-HER2* mice crossed with $BIM^{-/-}$ knockout mice, tumors did not regress upon *MMTV-HER2* inactivation (14). These studies elegantly demonstrated the importance of a BCL-2 family member-mediated apoptotic response upon HER2 inhibition in *HER2*-amplified breast cancer.

Clinically, despite their clear benefit in the adjuvant setting (62), HER2 inhibitors have shown only modest activity as single agents (63). This is somewhat surprising given that RTK-addicted cancers in other solid tumor types are effectively treated with RTK inhibitor monotherapies (4, 64, 65). Given the demonstrated role of apoptosis in targeted therapy efficacy (reviewed in ref. 8), we reasoned that there may be a widespread deficiency in the HER2 inhibitor-induced apoptotic response.

Surprisingly, we uncovered that coamplification of the HER2 intronic miRNA, *miR-4728*, is responsible for depressed NOXA expression. We demonstrated that while blocking *miR-4728* increases phosphorylation and activation of ERK, as previously demonstrated (38), it also leads to up-regulation of ER and NOXA. Thus, our data point to a dual role for *miR-4728*: as a tumor antagonistic gene through down-regulation of pERK (38) and as an antagonist of HER2 inhibitor therapy by suppression of NOXA. Importantly, since HER2 inhibitors like lapatinib block ERK signaling in *HER2*-amplified breast cancers (Figs. 4 *D* and *E* and 5 and Figs. S6*A*, S8*B*, S11*B*, and S12, and ref. 9), it is likely that *miR-4728* only has an antagonistic effect in the presence of HER2 inhibitors, while *miR-4728* likely promotes tumorigenesis in the absence of HER2 inhibition. Indeed, we provide evidence that coamplification of *miR-4728* plays a role

in the lack of responses to HER2 inhibitors (Fig. 4). Moreover, the lack of single agent efficacy of HER2-targeting therapeutic antibodies, like trastuzumab (Herceptin) (66), might also be at least partly explained by down-regulation of NOXA expression. However, since trastuzumab-mediated cytotoxicity includes function outside of HER2 pathway inhibition (67, 68), the relationship between deficient NOXA and trastuzumab efficacy may differ. Importantly, however, Merino et al. (57) demonstrated robust activity of trastuzumab and S63845 in a *HER2*-amplified PDX model.

More globally, these data reveal that for kinases activated by focal amplification and treated with therapies targeting that kinase, a thorough understanding of coamplified genes may inform treatment strategies. In this case, amplification of *miR-4728* informs that *HER2*-amplified breast cancers should be treated with a HER2 inhibitor and a MCL-1 inhibitor. This may be particularly relevant for patients with high HER2 copy number as well as HER2+/ER− patients that have the lowest levels of NOXA (Fig. 2*A*).

Direct MCL-1 inhibitors are now being developed, reflecting the growing understanding of the importance of MCL-1 in cancer. A1210477 was the first widely tested, specific MCL-1 inhibitor. Underlying the emerging importance of MCL-1 in breast cancer, Xiao et al. (53) demonstrated that A1210477 has single-agent activity in a subset of breast cancers, including *HER2*-amplified breast cancer cell lines. Similar to our findings, the disruption of MCL-1:BIM complexes was reported as a major mechanism of A1210477 efficacy, and BIM reduction by siRNA markedly mitigated the efficacy of the agent. They also noted that MCL-1 increased in whole-cell lysates of SKBR3 cells following A1210477 treatment, similar to our findings (Fig. S8*A*). Moreover, they observed an increase in MCL-1:BAK complexes at lower concentrations (2.5 μM) of A1210477. Since it is already known that MCL-1 has a preference for binding to BAK over BAX (69), the disruption of MCL-1:BAK complexes is of significant importance for the induction of apoptosis, which we achieved with S63845 (Fig. 5*E*) and could explain why we saw a larger amount of BAK activation after treatment with S63845 vs. A1210477 (Fig. 5*D*).

Both selective MCL-1 inhibitors used in our study function as derepressors by displacing proapoptotic BCL-2 family proteins from MCL-1. They both increase MCL-1 levels, likely by inhibiting the interaction of MCL-1 with proteins such as NOXA that facilitate proteasomal degradation (43, 56). Over the last 10 y, several models have been developed to investigate the dependence of different types of cancer on the antiapoptotic BCL-2 family proteins for survival (70). Our data support that the observed sensitivity of *HER2*-amplified breast cancer cell lines to MCL-1 inhibition in the presence of lapatinib was BIM-, BAK-, but also BAX-dependent, since silencing these three proapoptotic BCL-2 family members significantly rescued the cells from apoptosis. It should be noted that BIM knockdown and BAX knockdown seemed redundant (Fig. S11*B*), consistent with BIM preferentially activating BAX to kill (49, 71). Our data, therefore, highlight the importance of both displacement of BIM from the prosurvival BCL-2 family proteins (to activate BAX) and displacement of BAK from MCL-1.

While this manuscript was in preparation, Merino et al. (57) demonstrated that S63845 and the HER2-directed antibody trastuzumab combined to induce marked antitumor activity in *HER2*-amplified breast cancer. Their treatment schedule differed from ours: Merino et al. treated mice once a week with S63845, demonstrating that long-term use of the combination (60 d) is both tolerable and efficacious. Our data also support the use of this combination in vivo (Fig. 6 and Fig. S13), and the sum of our work provides a mechanistic rationale for its implementation. Furthermore, as we found that *NOXA* (*PMAIP1*) mRNA levels are lowest in the *HER2*-amplified/ER− subgroup of human breast tumors (Fig. 2*A*), this subgroup of patients may benefit the most from combined targeting of HER2 and MCL-1. These findings may have further implications, as we also report NOXA was among the most highly down-regulated genes following treatment of ER+ breast cancers with the antiaromatase letrozole (Fig. 2*D*), which we recapitulated in vitro (Fig. S4*B*). These data suggest these breast cancers may also acquire a reliance on MCL-1 as treatment progresses with antiestrogen drugs, and our future work will focus on delineating this precise point.

Overall, our study uncovers an important role for an amplified miRNA within the *17q12-21* amplicon, driving resistance to HER2 inhibitors. This study represents an example of a coamplified gene that mitigates response to a kinase inhibitor within the same amplicon that created the kinase addiction in the first place. It also highlights difficulties that may arise when targeting an oncogene within a cancer-addicted amplicon with a targeted therapeutic—difficulties that do not arise when the addictive oncogene is mutated or translocated, as in the case of *EGFR*-mutant and *ALK*-translocated lung cancers. This fundamental difference would appear to contribute to the differential efficacy of these drugs compared with HER2 inhibitors, and analogous situations may arise in other cancers addicted to oncogenes that are activated by amplification.

Materials and Methods

Cell Lines. The cell lines in this study were from the Massachusetts General Hospital. SKBR3, BT-474, MDA-MB-231, MDA-MB-468, and BT-549 cells were grown in DMEM/F12 (HyClone Laboratories, Inc.) with 10% FBS in the presence of 1 μg/mL penicillin and streptomycin. MDA-MB-361, MDA-MB-453, HCC-1419, UACC-893, HCC-1395, HCC-1937, and HCC-38 cells were cultured in RPMI with 10% FBS in the presence of 1 μg/mL penicillin and streptomycin. UACC-812, CAL-120, MCF-7, and 293T cells were cultured in DMEM with 10% FBS in the presence of antibiotics. EFM-192A cells were grown in RPMI with 20% FBS in the presence of 1 μg/mL penicillin and streptomycin.

Reagents and Antibodies. The following drugs were kindly provided by Abbvie: venetoclax, A1210477, and A1331852. The following drugs were purchased: S63845 for in vitro and in vivo studies (S-63845; Chemietek), Lapatinib Ditosylate (Tykerb) for in vitro and in vivo studies (M1802; Abmole), and Fulvestrant (S1191; Selleckchem).

The antibodies used in this study (clone/cat. no.) were as follows: Anti-Bak (Ab-1 clone for IP) (AM03; EMD Millipore), anti-BAX (6A7 clone for IP) (sc-23959; Santa Cruz), anti-BAX (*N*-20 clone) (sc-493; Santa Cruz), anti-Bak (3814S; Cell Signaling), anti-Bim (C34C5) (2933S; Cell Signaling), anti-Noxa (D8L7U) (14766S; Cell Signaling), anti–Bcl-2 (D55G8) (Human Specific) (4223S; Cell Signaling), anti-Cleaved PARP (Asp214) (D64E10) (5625S; Cell Signaling), anti-GAPDH (6C5) (sc-32233; Santa Cruz), anti-HER2/ErbB2 (29D8) (2165S; Cell Signaling), anti–MCL-1 (S-19) (sc-819; Santa Cruz), anti–BCL-xL (54H6) (2764S; Cell Signaling), 4E-BP1 (53H11) (9644S; Cell Signaling), phospho-4E-BP1 (Thr37/46) (236B4) (2855S; Cell Signaling), anti–Phospho-S6 Ribosomal Protein (Ser240/244) (D68F8) (5364S; Cell Signaling), anti–Phospho-Akt (Thr308) (244F9) (4056S; Cell Signaling), anti-ERα (D8H8) (8644S; Cell Signaling), anti–Phospho-HER2/ErbB2 (Tyr1248) (2247S; Cell Signaling), anti-Akt (C67E7) (4691S; Cell Signaling), anti-cleaved Caspase-3 (Asp175) (5A1E; Cell Signaling), Normal Rabbit IgG for IP (sc-2027; Santa Cruz), and Normal Mouse IgG for IP (sc-2025; Santa Cruz).

All mouse experiments were approved and performed in accordance with the Institutional Animal Care and Use Committee at Virginia Commonwealth University (VCU).

ACKNOWLEDGMENTS. We thank Dr. Mario Acunzo for helpful discussions on miRNA function. Services and products in support of the research project were generated by the VCU Massey Cancer Center Cancer Mouse Model Shared Resource, supported, in part, with funding from NIH–NCI Cancer Center Support Grant P30 CA016059. This work is supported by NCI Career Development Award K22 CA175276 and Mary Kay Foundation Grant 017-75 (to A.C.F.). J.A. is supported by the Breast Cancer Research Foundation (BCRF-17-008), Instituto de Salud Carlos III (PI16/00253), and Spanish Association Against Cancer (AECC). We acknowledge "Tumor Biomarkers Collaboration" supported by the Banco Bilbao Vizcaya Argentaria (BBVA) Foundation (to M.S. and V.S.) and the "la Caixa" Foundation. V.S. is also supported by the Miguel Servet Program (ISCIII, CP14/00228). M.S. was funded by NIH Grant P30CA008748 and the Breast Cancer Research Foundation.

1. Slamon DJ, et al. (2001) Use of chemotherapy plus a monoclonal antibody against HER2 for metastatic breast cancer that overexpresses HER2. *N Engl J Med* 344: 783–792.
2. Viani GA, Afonso SL, Stefano EJ, De Fendi LI, Soares FV (2007) Adjuvant trastuzumab in the treatment of her-2-positive early breast cancer: A meta-analysis of published randomized trials. *BMC Cancer* 7:153.
3. Baselga J, et al. (2005) Phase II study of efficacy, safety, and pharmacokinetics of trastuzumab monotherapy administered on a 3-weekly schedule. *J Clin Oncol* 23: 2162–2171.
4. Sequist LV, et al. (2008) First-line gefitinib in patients with advanced non-small-cell lung cancer harboring somatic EGFR mutations. *J Clin Oncol* 26:2442–2449.
5. Shaw AT, et al. (2013) Crizotinib versus chemotherapy in advanced ALK-positive lung cancer. *N Engl J Med* 368:2385–2394.
6. Faber AC, et al. (2009) Differential induction of apoptosis in HER2 and EGFR addicted cancers following PI3K inhibition. *Proc Natl Acad Sci USA* 106:19503–19508.
7. Friboulet L, et al. (2014) The ALK inhibitor ceritinib overcomes crizotinib resistance in non-small cell lung cancer. *Cancer Discov* 4:662–673.
8. Hata AN, Engelman JA, Faber AC (2015) The BCL2 family: Key mediators of the apoptotic response to targeted anticancer therapeutics. *Cancer Discov* 5:475–487.
9. Faber AC, et al. (2011) BIM expression in treatment-naive cancers predicts responsiveness to kinase inhibitors. *Cancer Discov* 1:352–365.
10. Montero J, et al. (2015) Drug-induced death signaling strategy rapidly predicts cancer response to chemotherapy. *Cell* 160:977–989.
11. Costa C, et al. (2014) The impact of EGFR T790M mutations and BIM mRNA expression on outcome in patients with EGFR-mutant NSCLC treated with erlotinib or chemotherapy in the randomized phase III EURTAC trial. *Clin Cancer Res* 20:2001–2010.
12. Ng KP, et al. (2012) A common BIM deletion polymorphism mediates intrinsic resistance and inferior responses to tyrosine kinase inhibitors in cancer. *Nat Med* 18:521–528.
13. Hata AN, et al. (2014) Failure to induce apoptosis via BCL-2 family proteins underlies lack of efficacy of combined MEK and PI3K inhibitors for KRAS-mutant lung cancers. *Cancer Res* 74:3146–3156.
14. Bean GR, et al. (2013) PUMA and BIM are required for oncogene inactivation-induced apoptosis. *Sci Signal* 6:ra20.
15. Ham J, et al. (2016) Exploitation of the apoptosis-primed state of MYCN-amplified neuroblastoma to develop a potent and specific targeted therapy combination. *Cancer Cell* 29:159–172.
16. Cang S, Iragavarapu C, Savooji J, Song Y, Liu D (2015) ABT-199 (venetoclax) and BCL-2 inhibitors in clinical development. *J Hematol Oncol* 8:129.
17. Nakagawa T, et al. (2013) EGFR-TKI resistance due to BIM polymorphism can be circumvented in combination with HDAC inhibition. *Cancer Res* 73:2428–2434.
18. Barretina J, et al. (2012) The Cancer Cell Line Encyclopedia enables predictive modelling of anticancer drug sensitivity. *Nature* 483:603–607.
19. Chin K, et al. (2006) Genomic and transcriptional aberrations linked to breast cancer pathophysiologies. *Cancer Cell* 10:529–541.
20. Bonnefoi H, et al. (2007) Validation of gene signatures that predict the response of breast cancer to neoadjuvant chemotherapy: A substudy of the EORTC 10994/BIG 00-01 clinical trial. *Lancet Oncol* 8:1071–1078.
21. Richardson AL, et al. (2006) X chromosomal abnormalities in basal-like human breast cancer. *Cancer Cell* 9:121–132.
22. Lu X, et al. (2008) Predicting features of breast cancer with gene expression patterns. *Breast Cancer Res Treat* 108:191–201.
23. Sotiriou C, et al. (2003) Breast cancer classification and prognosis based on gene expression profiles from a population-based study. *Proc Natl Acad Sci USA* 100: 10393–10398.
24. Kao KJ, Chang KM, Hsu HC, Huang AT (2011) Correlation of microarray-based breast cancer molecular subtypes and clinical outcomes: Implications for treatment optimization. *BMC Cancer* 11:143.
25. Anonymous; Cancer Genome Atlas Network (2012) Comprehensive molecular portraits of human breast tumours. *Nature* 490:61–70.
26. Rhodes DR, et al. (2004) ONCOMINE: A cancer microarray database and integrated data-mining platform. *Neoplasia* 6:1–6.
27. Su D, et al. (2012) Role of ERRF, a novel ER-related nuclear factor, in the growth control of ER-positive human breast cancer cells. *Am J Pathol* 180:1189–1201.
28. Liu W, Swetzig WM, Medisetty R, Das GM (2011) Estrogen-mediated upregulation of Noxa is associated with cell cycle progression in estrogen receptor-positive breast cancer cells. *PLoS One* 6:e29466.
29. Sabatier R, et al. (2011) A gene expression signature identifies two prognostic subgroups of basal breast cancer. *Breast Cancer Res Treat* 126:407–420.
30. Onitilo AA, Engel JM, Greenlee RT, Mukesh BN (2009) Breast cancer subtypes based on ER/PR and Her2 expression: Comparison of clinicopathologic features and survival. *Clin Med Res* 7:4–13.
31. Miller WR, Larionov A, Anderson TJ, Evans DB, Dixon JM (2012) Sequential changes in gene expression profiles in breast cancers during treatment with the aromatase inhibitor, letrozole. *Pharmacogenomics J* 12:10–21.
32. Yuan G, et al. (2008) HER2-dependent MMP-7 expression is mediated by activated STAT3. *Cell Signal* 20:1284–1291.
33. Kim YK, Kim VN (2007) Processing of intronic microRNAs. *EMBO J* 26:775–783.
34. Persson H, et al. (2011) Identification of new microRNAs in paired normal and tumor breast tissue suggests a dual role for the ERBB2/Her2 gene. *Cancer Res* 71:78–86.
35. Moasser MM (2007) The oncogene HER2: Its signaling and transforming functions and its role in human cancer pathogenesis. *Oncogene* 26:6469–6487.
36. Newie I, et al. (2016) HER2-encoded mir-4728 forms a receptor-independent circuit with miR-21-5p through the non-canonical poly(A) polymerase PAPD5. *Sci Rep* 6:35664.
37. Newie I, et al. (2014) The HER2-encoded miR-4728-3p regulates ESR1 through a non-canonical internal seed interaction. *PLoS One* 9:e97200.
38. Schmitt DC, et al. (2015) ErbB2-intronic microRNA-4728: A novel tumor suppressor and antagonist of oncogenic MAPK signaling. *Cell Death Dis* 6:e1742.
39. Speirs V, et al. (1999) Coexpression of estrogen receptor alpha and beta: Poor prognostic factors in human breast cancer? *Cancer Res* 59:525–528.
40. Osborne CK, Wakeling A, Nicholson RI (2004) Fulvestrant: An oestrogen receptor antagonist with a novel mechanism of action. *Br J Cancer* 90(Suppl 1):S2–S6.
41. Chen L, et al. (2005) Differential targeting of prosurvival Bcl-2 proteins by their BH3-only ligands allows complementary apoptotic function. *Mol Cell* 17:393–403.
42. Beroukhim R, et al. (2010) The landscape of somatic copy-number alteration across human cancers. *Nature* 463:899–905.
43. Leverson JD, et al. (2015) Potent and selective small-molecule MCL-1 inhibitors demonstrate on-target cancer cell killing activity as single agents and in combination with ABT-263 (navitoclax). *Cell Death Dis* 6:e1590.
44. Serra V, et al. (2011) PI3K inhibition results in enhanced HER signaling and acquired ERK dependency in HER2-overexpressing breast cancer. *Oncogene* 30:2547–2557.
45. Leverson JD, et al. (2015) Exploiting selective BCL-2 family inhibitors to dissect cell survival dependencies and define improved strategies for cancer therapy. *Sci Transl Med* 7:279ra40.
46. Chipuk JE, Green DR (2008) How do BCL-2 proteins induce mitochondrial outer membrane permeabilization? *Trends Cell Biol* 18:157–164.
47. Chipuk JE, Moldoveanu T, Llambi F, Parsons MJ, Green DR (2010) The BCL-2 family reunion. *Mol Cell* 37:299–310.
48. Llambi F, et al. (2011) A unified model of mammalian BCL-2 protein family interactions at the mitochondria. *Mol Cell* 44:517–531.
49. Kim H, et al. (2009) Stepwise activation of BAX and BAK by tBID, BIM, and PUMA initiates mitochondrial apoptosis. *Mol Cell* 36:487–499.
50. O'Neill KL, Huang K, Zhang J, Chen Y, Luo X (2016) Inactivation of prosurvival Bcl-2 proteins activates Bax/Bak through the outer mitochondrial membrane. *Genes Dev* 30:973–988.
51. Tanizaki J, et al. (2011) Roles of BIM induction and survivin downregulation in lapatinib-induced apoptosis in breast cancer cells with HER2 amplification. *Oncogene* 30:4097–4106.
52. Certo M, et al. (2006) Mitochondria primed by death signals determine cellular addiction to antiapoptotic BCL-2 family members. *Cancer Cell* 9:351–365.
53. Xiao Y, et al. (2015) MCL-1 is a key determinant of breast cancer cell survival: Validation of MCL-1 dependency utilizing a highly selective small molecule inhibitor. *Mol Cancer Ther* 14:1837–1847.
54. Faber AC, et al. (2014) mTOR inhibition specifically sensitizes colorectal cancers with KRAS or BRAF mutations to BCL-2/BCL-XL inhibition by suppressing MCL-1. *Cancer Discov* 4:42–52.
55. Faber AC, et al. (2015) Assessment of ABT-263 activity across a cancer cell line collection leads to a potent combination therapy for small-cell lung cancer. *Proc Natl Acad Sci USA* 112:E1288–E1296.
56. Kotschy A, et al. (2016) The MCL1 inhibitor S63845 is tolerable and effective in diverse cancer models. *Nature* 538:477–482.
57. Merino D, et al. (2017) Synergistic action of the MCL-1 inhibitor S63845 with current therapies in preclinical models of triple-negative and HER2-amplified breast cancer. *Sci Transl Med* 9:eaam7049.
58. Griffiths GJ, et al. (1999) Cell damage-induced conformational changes of the pro-apoptotic protein Bak in vivo precede the onset of apoptosis. *J Cell Biol* 144:903–914.
59. Hsu YT, Youle RJ (1997) Nonionic detergents induce dimerization among members of the Bcl-2 family. *J Biol Chem* 272:13829–13834.
60. Baselga J, et al. (1999) Phase II study of weekly intravenous trastuzumab (Herceptin) in patients with HER2/neu-overexpressing metastatic breast cancer. *Semin Oncol* 26(Suppl 12):78–83.
61. Moody SE, et al. (2002) Conditional activation of Neu in the mammary epithelium of transgenic mice results in reversible pulmonary metastasis. *Cancer Cell* 2:451–461.
62. Gianni L, et al. (2010) Neoadjuvant chemotherapy with trastuzumab followed by adjuvant trastuzumab versus neoadjuvant chemotherapy alone, in patients with HER2-positive locally advanced breast cancer (the NOAH trial): A randomised controlled superiority trial with a parallel HER2-negative cohort. *Lancet* 375:377–384.
63. Baselga J, et al. (1996) Phase II study of weekly intravenous recombinant humanized anti-p185HER2 monoclonal antibody in patients with HER2/neu-overexpressing metastatic breast cancer. *J Clin Oncol* 14:737–744.
64. Shaw AT, et al. (2011) Effect of crizotinib on overall survival in patients with advanced non-small-cell lung cancer harbouring ALK gene rearrangement: A retrospective analysis. *Lancet Oncol* 12:1004–1012.
65. Sawyers CL, et al. (2002) Imatinib induces hematologic and cytogenetic responses in patients with chronic myelogenous leukemia in myeloid blast crisis: Results of a phase II study. *Blood* 99:3530–3539.
66. Pohlmann PR, Mayer IA, Mernaugh R (2009) Resistance to trastuzumab in breast cancer. *Clin Cancer Res* 15:7479–7491.
67. Garcia-Garcia C, et al. (2012) Dual mTORC1/2 and HER2 blockade results in antitumor activity in preclinical models of breast cancer resistant to anti-HER2 therapy. *Clin Cancer Res* 18:2603–2612.
68. Scaltriti M, et al. (2009) Lapatinib, a HER2 tyrosine kinase inhibitor, induces stabilization and accumulation of HER2 and potentiates trastuzumab-dependent cell cytotoxicity. *Oncogene* 28:803–814.
69. Willis SN, et al. (2005) Proapoptotic Bak is sequestered by Mcl-1 and Bcl-xL, but not Bcl-2, until displaced by BH3-only proteins. *Genes Dev* 19:1294–1305.
70. Deng J, et al. (2007) BH3 profiling identifies three distinct classes of apoptotic blocks to predict response to ABT-737 and conventional chemotherapeutic agents. *Cancer Cell* 12:171–185.
71. Sarosiek KA, et al. (2013) BID preferentially activates BAK while BIM preferentially activates BAX, affecting chemotherapy response. *Mol Cell* 51:751–765.